Ca-Doped Strontianite−Calcite Hybrid Micropillar Arrays Formed via Oriented Dissolution and Heteroepitaxial Growth on Calcite

Weike Wu,[†,‡] Yurong Ma,*[,†] Ying Xing,[§] Yuzhe Zhang,[†] Heng Yang,[†] Qiang Luo,[§] Jian Wang,[§] Bin Li,*[,‡] and Limin Qi[†]

[†]Beijing National Laboratory for Molecular Sciences (BNLMS), State Key Laboratory for Structural Chemistry of Unstable and Stable Species, College of Chemistry, Peking University, Beijing 100871, P.R. China
[‡]School of Chemistry and Chemical Engineering, Guangxi University, Nanning 530004, China
[§]International Center for Quantum Materials, School of Physics, Peking University, Beijing 100871, China

Ⓢ *Supporting Information*

ABSTRACT: Even though heteroepitaxial growth of one-dimensional microstructures or three-dimensional islands has been realized via strategies such as chemical vapor deposition, molecular beam epitaxy, and solution phase, researchers have not succeeded in the formation of one-dimensional hybrid microstructures via the combination of heteroepitaxial growth and oriented dissolution up to now. In this work, well ordered single crystalline calcium-doped strontianite−calcite hybrid micropillar arrays with the long axis along the [001] direction of the two phases were formed on calcite (104) substrates via heteroepitaxial growth of strontianite and oriented dissolution of calcite in aqueous solution for the first time. Energy-dispersive spectroscopy analysis shows that the micropillars are composed of strontianite occluded with about 12 mol % of Ca. During the growth process of strontianite, calcite cores formed in the inner side of the strontianite micropillars at the base stage via the oriented dissolution. The lattices of the strontianite and calcite match very well at the interface of calcite and strontianite. A novel formation mechanism is proposed for the formation of Ca-doped strontianite−calcite hybrid micropillars via the synergetic process of the oriented dissolution of one carbonate mineral and the heteroepitaxial growth of another carbonate mineral in Volmer−Weber growth mode with a small lattice misfit. Ca-doped strontianite micropillar arrays might grow epitaxially on the calcite (001) and (104) planes with small misfits.
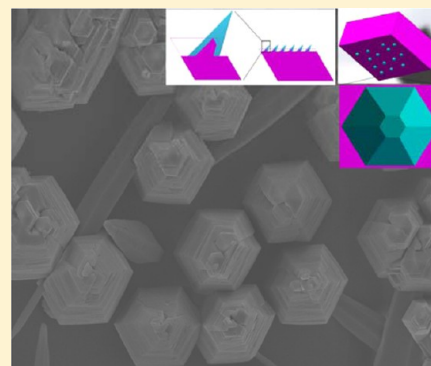
INTRODUCTION

Epitaxy means order in the relative orientation of identical crystals nucleated and grown on a large single crystal face.[1] Every crystal of the deposited material is oriented in such a way that there is coincidence of some vectors of its reciprocal lattice with vectors of the reciprocal lattice of the substrate surface. Heteroepitaxial growth should lead to formation and growth of either layer-by-layer growth (Frank−van der Merwe mode), layer-by-layer growth followed by three-dimensional (3D) islands (Stranski−Krastanov mode), and 3D islands (Volmer−Weber mode) depending on the values of the lattice misfit.[1−3] Secondary nucleation and epitaxial growth of one mineral on another one may proceed when they have similar lattice properties, which are important issues in crystallography, mineralogy, geochemistry, and materials science. For example, one-dimensional (1D) heteroepitaxy can accommodate mismatch strain through lateral strain relaxation, allowing single crystalline 1D nanostructures of metals and semiconductors such as Ge nanopillar arrays,[4,5] Pd pyramids,[6] In$_x$Ga$_{1−x}$As,[7] In$_x$Ga$_{1−x}$N,[8] and ZnO nanowires[9] epitaxially grown on substrates with as much as 46% lattice mismatch. All the above-mentioned 1D nanostructures were epitaxially grown on

single crystalline substrates via strategies such as chemical vapor deposition (CVD),[5,7] molecular beam epitaxy (MBE),[6,8,10] vapor liquid solid (VLS),[4,10] and solution phase.[9] Reactions at mineral−fluid interfaces play a key role in processes ranging from the deep earth to materials synthesis and nuclear waste storage.[11] An interface-coupled dissolution−precipitation mechanism can transfer crystallographic information via structural matching (epitaxy) when the product nucleates on the parent substrates.[12] In the presence of a fluid phase, mineral conversion from one rock type to another turns out to proceed through dissolution and recrystallization at the mineral−fluid interface.[13] Epitaxial growth of metal carbonates on the calcite or dolomite (104) face has been reported in the last few years. These crystal phases may be represented by differently composed members of a solid solution, e.g., Mg$_x$Ca$_{1−x}$CO$_3$,[14,15] or by two different species such as CdCO$_3$[16] on calcite substrates. Epitaxial growth of magnesium calcite[14] with nanometer dimensions on the (104) surface of calcite has

been observed in solution by using in situ atomic force microscopy (AFM).[13] In situ AFM results indicate that the heteroepitaxial growth of 3D islands of $CdCO_3$ on the calcite (104) face proceeds via three different mechanisms: advancement of existing steps, nucleation and growth of 3D islands, and nucleation and spread of 2D nuclei, depending on the initial supersaturation of the aqueous solution.[16] It was reported that aragonite grew on all faces of strontianite with 4.5% average epitaxial strain and on the (001) face of $PbCO_3$ with 5.4% epitaxial strain.[17] Recently, we realized the heteroepitaxial growth of single crystalline witherite ($BaCO_3$) microcone arrays on calcite (104) face via a dissolution–epitaxial growth reaction.[18] However, the crystalline planes for the epitaxial growth frontier and the growth interface of the two carbonate minerals were not characterized in the witherite–calcite system.[18]

Aragonite-type $SrCO_3$, strontianite, has been applied in a wide field such as biosensors, cathode ray tubes for televisions and computer monitors, pyrotechnics, an additive for special glass, a component in ferrite magnets, and a precursor for various strontium compounds.[19] Strontianite with different morphologies such as spheres and ellipsoids,[20,21] core–shell spheres,[22] olive-like and flower-like nanostructures,[23,24] and 1D nanostructures[19,25,26] have been synthesized via several methods. As for the obtained single crystalline one-dimensional micro- and nanostructures of strontianite, the long axis of strontianite could be along [001],[17] unknown directions,[20,21,25,26] or not along any defined crystallographic axis.[19] Even though 1D strontianite micro- or nanostructures have been synthesized via a few different methods, none of the ordered arrays of 1D strontianite have been reported, to the best of our knowledge.

It was suggested that nacreous aragonite evolved through simple horizontal partitioning of vertical calcitic prisms.[27] Cheta and co-workers found that the crystallographic c-axis of nacreous aragonite tablets inherits the crystallographic orientation of the most distal fibers of calcitic prisms, which act as epitaxial mineral substrates.[28] If early nacre tablets grew epitaxially on calcitic prisms, all nacreous tablets on a single prism would display an even orientation (inherited from the calcitic prism). However, it is not the case since SEM observations indicated that early nacreous crystals were usually polycrystalline; they had a common c axis orientation but were randomly oriented in terms of axes a and b.[29] Olson et al.[30] also found that the nucleation of disordered spherulitic aragonite crystals occurs near the nacre–prism boundary, which is controversial to the horizontal partitioning hypothesis. Thus, it is still a dilemma whether there is heteroepitaxial growth of nacreous aragonite on calcitic prisms in mollusk shells. Heteroepitaxial growth of aragonite type polymorth, strontianite on calcite in this work may shed light on the growth process of the nacreous aragonite tablets on calcite prism layers in the mollusk shells.

Herein, well ordered single crystalline calcium-doped strontianite–calcite hybrid micropillar arrays with the long axis along the [001] direction were formed on a calcite (104) substrate via a synergetic process of oriented dissolution and heteroepitaxial growth in aqueous solution for the first time.

■ EXPERIMENTAL SECTION

Materials. Strontium nitrate was bought from Sinopharm Chemical Reagent Co. Ltd. (China) and was applied in the experiments without further treatment. Cleaved calcite (104) substrates were obtained by knocking down geological calcite single crystals and were thoroughly washed with double distilled water under ultrasonication more than three times until all the artifacts on the substrates were removed. These substrates were then dried and kept in a desiccator before use.

Epitaxial Growth of Calcium-Doped Strontianite on Calcite (104) Substrate. The concentration of strontium nitrate in the mixed solvents composed of 9 mL of double-distilled water and 1 mL of ethanol is 5 mM (if not otherwise indicated). Two calcite substrates with a size about $5 \times 5 \times 1$ mm^3 (104) plane were placed at the bottom of the beaker. The beaker was sealed by aluminum foil and parafilm and kept statically at 27 °C for 10 h (if not otherwise indicated). The calcite substrates were then taken out from the solutions and washed completely with double-distilled water for further characterizations.

Characterizations. Scanning electron microscopy (SEM) images were captured on Navo Nano 430 at an accelerating voltage of 1.0–10.0 kV. Top view and side view images were taken by tilting and rotating the sample holder together with the calcite substrates to appropriate positions under SEM instruments. The angle between the calcite [001] direction and the (104) plane is 45.4°. Therefore, we placed the calcite substrate with calcium strontianite micropillar arrays on a sample holder that has an angle of 45° to the horizontal plane.

To prepare the longtitudinal and transverse cross sections of the Ca-doped strontianite–calcite hybrid micropillars on calcite substrates, the samples were first embedded with resin. The longitudinal cross sections were then obtained after cutting along the calcite ($\bar{1}20$) plane by using a low speed saw, while the transverse cross sections were obtained via grinding along (104) plane with sandpapers.

Thin sections of the longitudinal cross section of Ca-doped strontianite-calcite hybrid micropillars were obtained by using focused ion beam etching and deposition system (FIB/SEM, FEI Helios NanoLab 600i) according to the following procedures. A protective layer of Pt with thickness about 1 μm was first formed by ion beam induced deposition onto a Ca-doped strontianite–calcite hybrid micropilar. A thin longitudinal section with thickness about 1.5 μm was obtained, transferred, and fixed onto a copper grid. Then the thin section was further thinned to be about 100 nm thick for transmission electron microscopy analysis.

Transmission electron microscope (TEM) images were recorded on a JEOL JEM-200CX at 160 kV. High resolution transmission electron microscope (HRTEM) images were captured on an FEI TECNAI F30 at 300 kV. X-ray diffraction (XRD) patterns of strontianite micropillar arrays on calcite substrates before and after epitaxial growth process were determined using a Rigaku Dmax-2000.

■ RESULTS AND DISCUSSION

Freshly cleaved calcite with exposed (104) planes was kept in 10 mL of mixed solvents of water and ethanol with 10 vol % of ethanol and with 5 mM of $Sr(NO_3)_2$ for 10 h at 27 °C. Conelike micropillars with clear side faces and edges can be seen on the calcite substrates from the scanning electron microscopy (SEM) images in Figure 1a–d, termed as side view images in the following text. Figure 1a indicates that the whole surface of the calcite substrate was covered with micropillars. In comparison, the top view image of the micropillars was obtained while tilting the sample holder until the electron beam was exactly parallel to the long axis of the micropillars (Figure 1e,f). Both of the side view (Figure 1c,d) and top view (Figure 1e,f) SEM images were taken from the same areas of calcite substrates; thus we can observe the same micropillars from different directions. The real length of the micropillars was calculated to be about 20–30 μm according to the side view SEM images in Figure 1a,b, considering the angle of the electron beam and the long axis of the micropillars. The top view images show pseudo-hexagonal projections with six sides and steps nearly parallel to each other (Figure 1e,f). As a
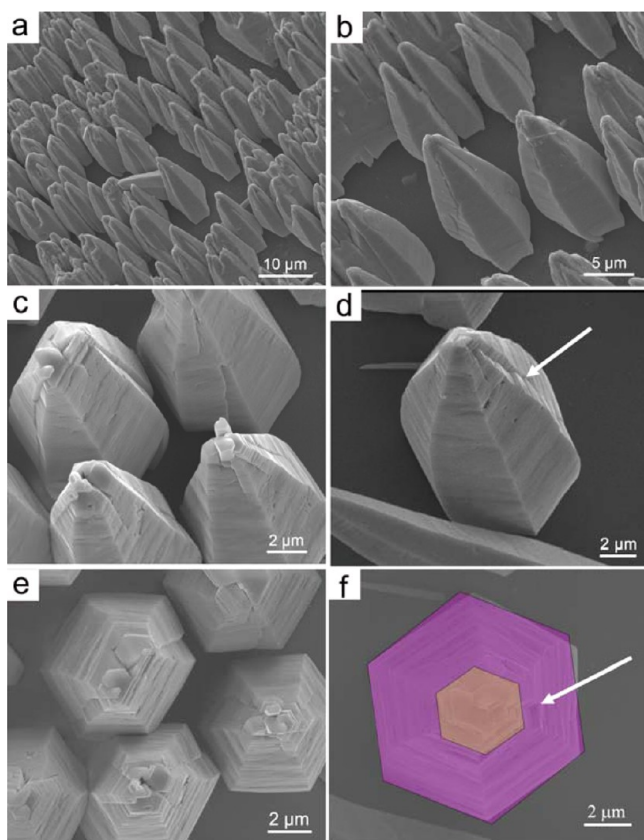
Figure 1. Side-view (a−d) and corresponding top-view (e, f) SEM images of the Ca-doped strontianite micropillar arrays epitaxially grown on calcite (104) face after 10 h in mixed solvents composed of 90 vol % of water and 10 vol % of ethanol at 27 °C. Note: The top-view SEM images were taken with the beamline parallel to the long axis of the micropillars, whereas the side view SEM images (a, b) and (c, d) were taken with the beamline some angles away from the long axis of the micropillars, 45° and 19°, respectively. As a comparison, the top view of one micropillar and the pink and brown hexagonal areas were put together in panel (f) to show the trisymmetrical feature of the micropillars.

comparison, the pink area focused on one micropillar exhibits two trisymmetrical hexagons, very close to the top view projection of the micropillar (Figure 1f).

Energy-dispersive spectroscopy (EDS) analysis on these micropillars indicates that they are composed of C, O, Ca, and Sr. The micropillars are composed of 12 ± 3 mol % of Ca and 88 ± 3 mol % of Sr if one considers the sum of the Ca mol % and the Sr mol % in the samples is 100% from the EDS analysis (Figure 2). The X-ray diffraction (XRD) pattern for the conelike micropillars on calcite substrates indicates that except the (104) diffraction peak of calcite, all the other diffraction peaks were indexed to strontianite, while the 2θ values of these peaks shift about 0.4−0.6° to higher values in comparison to the standard XRD pattern of strontianite[25] (JCPDS 05-0418) (Figure 3, Table S1, Supporting Information). Considering that the atomic radii for strontium is 145 pm, slightly bigger than that of calcium (132 pm),[31] the lattice distances for the strontianite doped with 12 mol % of calcium are slightly smaller than that for strontianite, and the diffraction peaks slightly shift to higher 2θ. According to the above EDS and XRD analysis, we conclude that the micropillars formed on calcite substrates are composed of Ca-doped strontianite in which about 12 ± 3

mol % of Ca took the site of Sr in the lattice structure. As one of the aragonite-type crystals, strontianite needles were reported to have pseudo-hexagonal cross section, and the characteristic supplementary angle between (110) and (1$\bar{1}$0) for the pseudo-hexagon is 117.5°,[17] similar to the pseudo-hexagonal structures observed from the top view SEM images (Figure 1e,f). There are always more than one clear groove-like stripe along the side faces of the micropillars from the zoomed-in SEM images (marked with white arrows, Figure 1d,f), which were probably formed during the heteroepitaxial growth process due to the lattice mismatch of strontianite and calcite substrate.

The elemental mapping image in Figure 2c clearly shows that there are small $CaCO_3$ protuberant cores (in pink) at the base of the $SrCO_3$ micropillar shells (in green). The calcite "cores" were exposed at the base stage of the micropillars when the micropillars were broken at the growth interface during the transformation of the samples (Figure 2b−e), probably due to the interface strain of $CaCO_3$ and $SrCO_3$. Nanomanipulation experiments demonstrated that calcite islands under compressive stress were easily detached from the dolomite (104) surfaces.[15] The calcite protuberant cores at the base of the $SrCO_3$ micropillars with elongated hexagonal steps can be seen more clearly after breaking some of the micropillars with a tweezer on purpose (Figure 2f). The elemental mapping images of the longitudinal cross sections of the strontianite micropillars clearly show that there are small calcite protuberant cores (in pink) at the base stage of the strontianite micropillar shells (in green, Figure 4). The angle between the long axis of the strontianite micropillars and the calcite (104) face is about 44.5° (Figure 4d), indicating that the long axis of the micropillars is almost parallel to the c-axis of calcite. The core−shell microstructures at the base of the micropillars are very obvious from the SEM and elemental mapping images of the transverse cross sections of the micropillars at the base stage (Figure S1, Supporting Information).

To get further information about the crystallographic direction of the Ca-doped strontianite micropillars on calcite substrates, thin sectioning for TEM analysis on the micropillars becomes a key issue. The size of Ca-doped strontianite micropillars in Figure 1 is too big for sectioning by using a commercial focused ion beam (FIB) etching and deposition system. Fortunately, well ordered micropillars with length about 2−3 μm were obtained after 1 h deposition time (Figure 5a), which were sectioned by using FIB and characterized under TEM. Figure 5b shows SEM images of the micropillar and its thin longitudinal cross section is parallel to the ($\bar{1}$20) plane before and after FIB, respectively. The light gray circumference in Figure 5c and the dark gray area on the left of the micropillar in Figure 5d (marked with a pink arrow) are Pt layer deposited on the surface of the micropillar for protection before FIB process. Selected area electron diffraction (SAED) pattern on the cubic area in Figure 5d indicates a single crystalline strontianite micropillar with its long axis parallel to the c axis of strontianite, consistent to all the area above the curved line with gray level difference of the micropillar (Figure 5d,e). In comparison, the area below the curved line shows diffraction patterns of calcite (Figure 5f). The small protuberance at the base stage of the micropillar in the TEM image is consistent with the observations from the SEM images in Figures 2 and 4. It can be concluded that the curved line actually exhibits the growth interface of strontianite on calcite substrate from the TEM image of the longitudinal cross
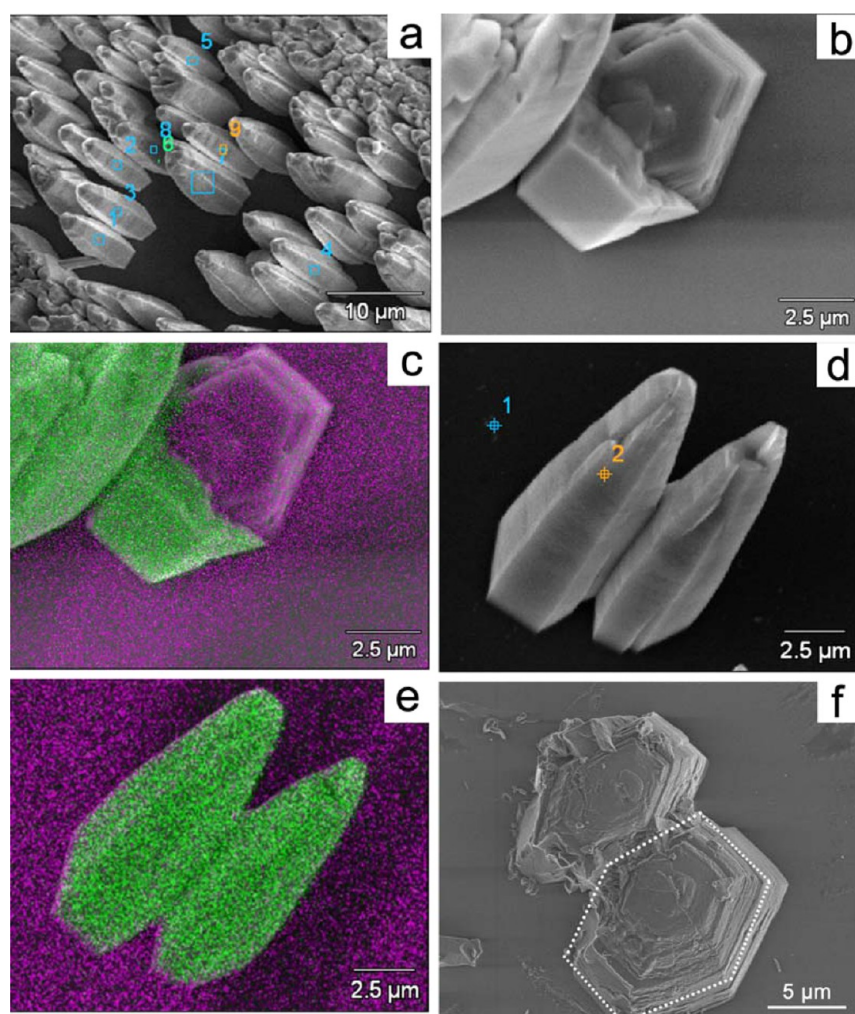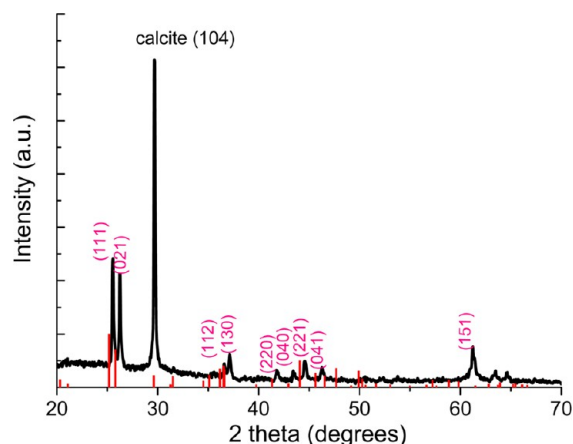
Figure 2. SEM and elemental mapping images of the Ca-doped strontianite-calcite hybrid micropillar arrays epitaxially grown on calcite (104) face after 10 h in mixed solvents composed of 90 vol % of water and 10 vol % of ethanol at 27 °C. (a) The elemental distribution on the cubic areas of the micropillars were characterized by EDS. The colors for the numbers in panels a and d were automatically set to indicate the cubic positions for EDS analysis, which cannot be changed afterward. (b–e) SEM images (b, d) and the relative elemental mapping images (c, e) on the same micropillars. The green and purple colors in the EDS mapping images (c, e) represent elements Sr and Ca, respectively. These colors were also automatically formed when the elemental mapping images were collected. (f) Some of the micropillars were broken on purpose with a tweezer, while all the samples were prepared as usual for the other SEM and elemental mapping images (a–e). These SEM images were obtained while the beamline is perpendicular to the (104) plane.

seciton of the micropillar in Figure 5d. The zone axes of the longitudinal cross section in Figure 5d are [010] and [100] for calcite and strontianite according to their SAED patterns, respectively.

The HRTEM image in Figure 5g shows that the lattice distances on the right-bottom area of the interface are 0.385 nm, 0.306 nm, 0.284 nm, 0.250 nm related to the (102), (104), (006), and (110) of calcite, respectively. On the contrary, the lattice distances on the left-up area of the interface are 0.797 nm, 0.577 nm, 0.468 nm, about 4.5–5% smaller than the lattice distances of (010), (001) of stronthianite (0.842 and 0.609 nm),[25] respectively, due to the replacement of 12 mol % of Sr by Ca, consistent with the XRD results. The crystal faces (001) and (010) of strontianite are parallel to (006) and (110) of calcite, respectively, while their related lattice distance values are close to multiple relationships. The epitaxial growth interface is almost parallel to the (104) plane of calcite from the HRTEM image.

The growth process of Ca-doped strontianite−calcite hybrid micropillars was tracked by characterizing the samples by using SEM after keeping the calcite substrate in the reaction solution for different times. Many micropillars with sizes from 500 nm to 2 μm were formed on the calcite (104) plane after keeping the calcite substrate in the reaction solution for 5 min (Figure 6a,b), indicating the fast nucleation and growth rates. One can also see a few hillocks with a size about 500 nm on the calcite substrate (Figure 6a). After 15 min, micropillars with heights about 3−5 μm can be seen from the SEM images (Figure 6c). Hillocks with layer-like microstructures can be seen on the calcite substrate from the zoomed-in image (Figure 6c). EDS analysis indicates that these hillocks are composed of calcite, while the micropillars are composed of $SrCO_3$ doped with about 13−26 mol % of calcium (Figure S2, Supporting Information). We propose that the hillocks observed at the early stage (5−15 min) were originally covered with micropillars which were removed from the calcite substrate during the sample transformation process. Denser and larger micro-
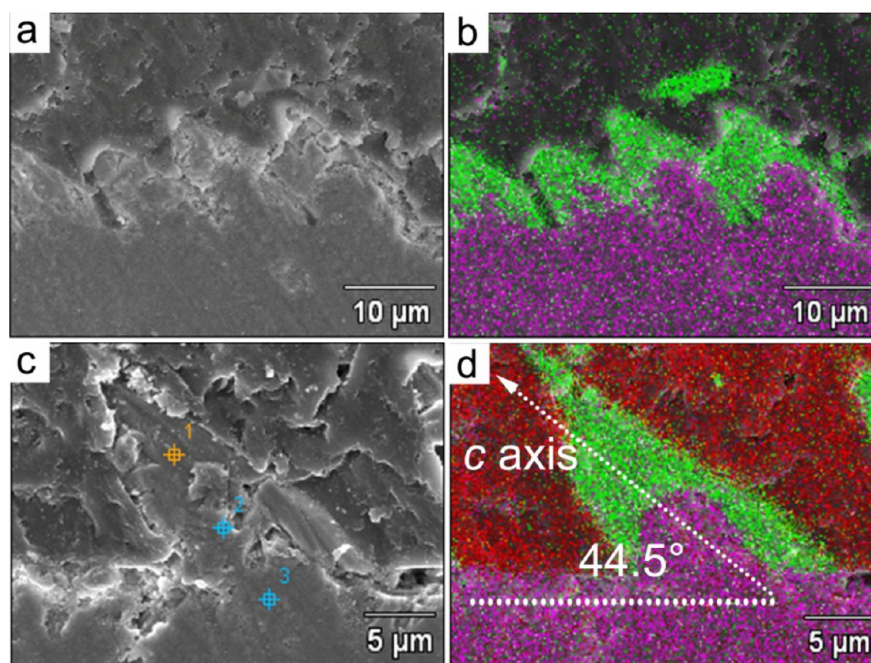
Figure 3. XRD pattern of the Ca-doped strontianite−calcite hybrid micropillar arrays formed on the calcite (104) face after 10 h in mixed solvents composed of 90 vol % of water and 10 vol % of ethanol at 27 °C. The red columns show the diffraction peaks of standard strontianite (JCPDS 05-0418).

pillars formed on the calcite substrate while extending the deposition time from 1 to 2 h (Figure 6d,e). After extending the reaction time to 30 h, the length for micropillars in Figure 1h increased to be more than 100 μm, while a lot of disordered microneedles formed on the surface of calcite (Figure 6f).

The influence of the experimental conditions such as precursor concentrations, the volume ratio of mixed solvents, and the reaction temperatures for the heteroepitaxial growth of Ca-doped strontianite micropillars was investigated in detail. Decreasing the concentration of $Sr(NO_3)_2$ from 5 mM to 1 mM, the calcite substrate was covered by a layer of calcite microneedles with a length about 1−2 μm and a small amount of strontianite micropillars with a length about 30 μm (Figure S3a,b). Thus, we propose that the formation of a small amount

of strontianite micropillars with a relatively large size at low $Sr(NO_3)_2$ concentration is probably attributed to the small amount of nuclei formed under low supersaturation degree for $SrCO_3$.

The formation of calcite microneedles is attributed to the anisotropic dissolution of calcite in unsaturated aqueous solution.[32,33] In comparison, a lot of epitaxially grown strontianite micropillars together with unaligned strontianite micropillars were formed on the calcite substrate at high $Sr(NO_3)_2$ concentration (10 mM) (Figure S3c,d). The influence of mixed solvents on the epitaxial growth of strontianite on calcite substrate was studied by changing the volume ratios of ethanol and water (Figure 7). Denser but smaller Ca-doped strontianite micropillars with sizes in the range of 6−12 μm formed while increasing the contents of ethanol in the mixed solvents from 0 to 20 vol % (Figure 7a−c). After further increasing the content of ethanol to 40 vol %, densely ordered and unaligned Ca-doped strontianite micropillars with a length of about 6 μm can be seen on the calcite (104) substrate (Figure 7d). The solubility of $SrCO_3$ in water at 25 °C is 0.023 g/100 mL H_2O.[34] Guo et al.[35] pointed out that $SrCO_3$ crystals can be easily and quickly precipitated even at 30 °C in a alcohol/water system, while no $SrCO_3$ crystal is detected in aqueous solution at a temperature below 50 °C, which suggests that alcohol favors the transformation of strontium dodecyl sulfate to $SrCO_3$ and accelerates the growth rate of $SrCO_3$ crystals. We assume the faster crystallization rate of $SrCO_3$ in the alcohol/water system is probably attributed to its lower solubility in the alcohol/water system than that in water. Decreasing the reaction temperature to 4 °C, walnut-like micropillars with corrugated side faces were formed on calcite (104) substrates (Figure S4a−c), very different from those formed at 27 °C. In comparison, the micropillars formed at higher temperature (50 °C) (Figure S4d−f) have bigger sizes and smoother side faces than those formed at 27 °C (Figure 1).


Figure 4. SEM and elemental mapping images for the longitudinal cross section of the Ca-doped strontianite-calcite hybrid micropillars obtained after cutting the samples along the calcite ($\bar{1}20$) plane. The green, purple, and red colors in the EDS mapping images (b, d) represent elements, Sr, Ca, and C, respectively. These colors were also automatically set when the elemental mapping images were collected.
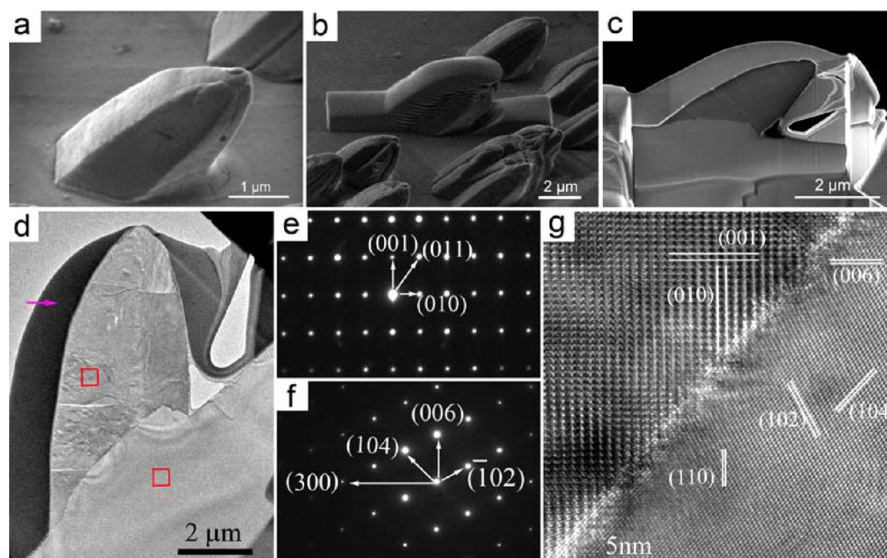
Figure 5. SEM (a−c) TEM (d), SAED (e, f), and HRTEM (g) images for the Ca-doped strontianite micropillars epitaxially grown on calcite (104) face after 1 h in mixed solvents composed of 90 vol % of water and 10 vol % of ethanol at 27 °C. The dark gray area on the left of the micropillar marked with a pink arrow in panel d are Pt layer deposited on the surface of the micropillar for protection before FIB process.
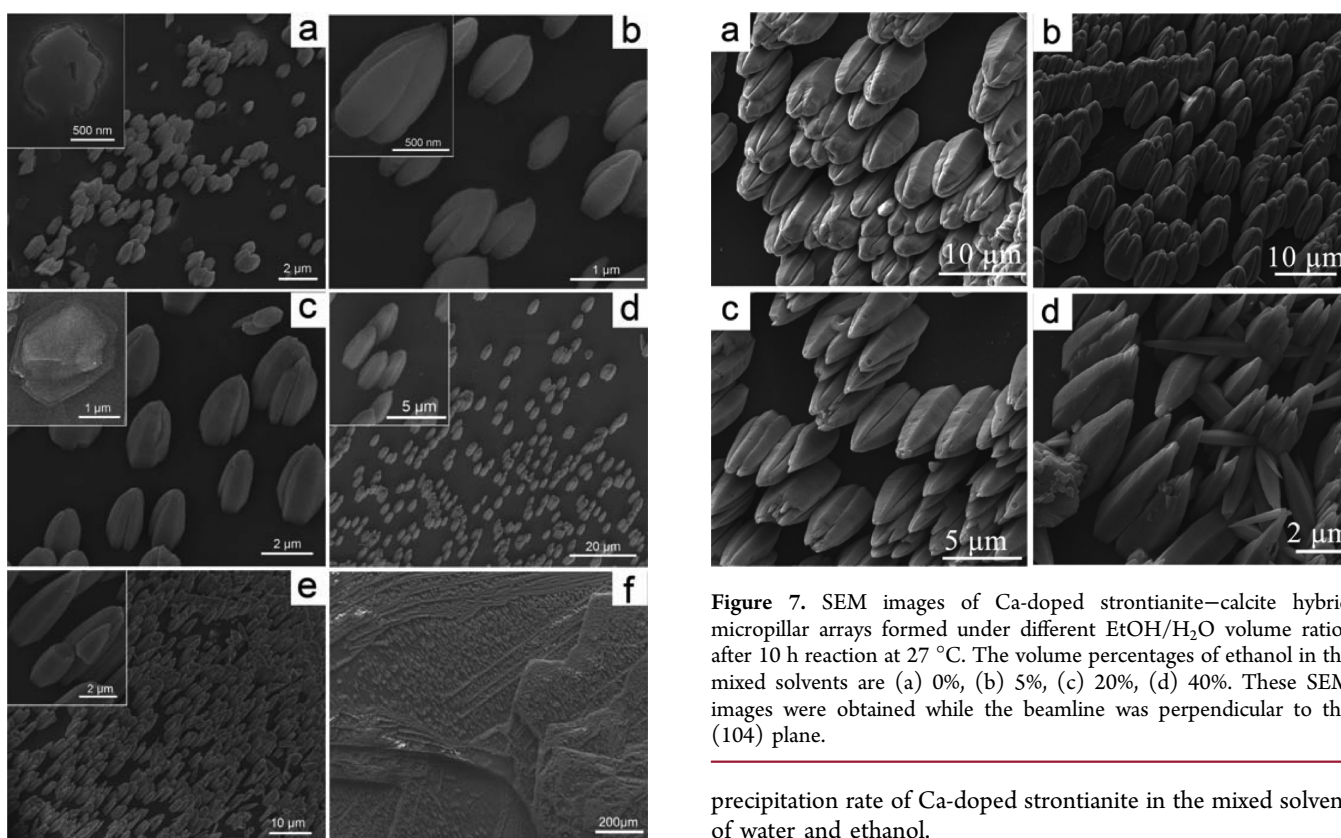
Figure 6. Side view SEM images of the Ca-doped strontianite micropillar arrays epitaxially grown on the calcite (104) face in mixed solvents composed of 90 vol % of water and 10 vol % of ethanol at 27 °C for different times. (a, b) 5 min; (c) 15 min; (d) 1 h, (e) 2 h, (f) 30 h. All the images were taken with the beamline 44.3° away from the *c* axis of calcite.

Figure 7. SEM images of Ca-doped strontianite−calcite hybrid micropillar arrays formed under different EtOH/H$_2$O volume ratios after 10 h reaction at 27 °C. The volume percentages of ethanol in the mixed solvents are (a) 0%, (b) 5%, (c) 20%, (d) 40%. These SEM images were obtained while the beamline was perpendicular to the (104) plane.

precipitation rate of Ca-doped strontianite in the mixed solvent of water and ethanol.

$$CaCO_3 + Sr^{2+} = Ca^{2+} + SrCO_3 \qquad (1)$$

In the witherite−calcite system, the growth interface was not known from experimental results in our previous study.[18] In this system, characterizations on the growth interface of strontianite on calcite were performed in detail by using TEM, SEM, and elemental analysis along transverse and longitudinal cross sections of the strontianite−calcite micropillars. The curved line in the TEM image of the longitudinal cross seciton of the micropillar in Figure 5d actually exhibits the growth interface of strontianite on calcite substrate. On the

The differences for the morphologies and sizes of the obtained Ca-doped strontianite formed at different temperatures are probably related to the variations of solubility and the
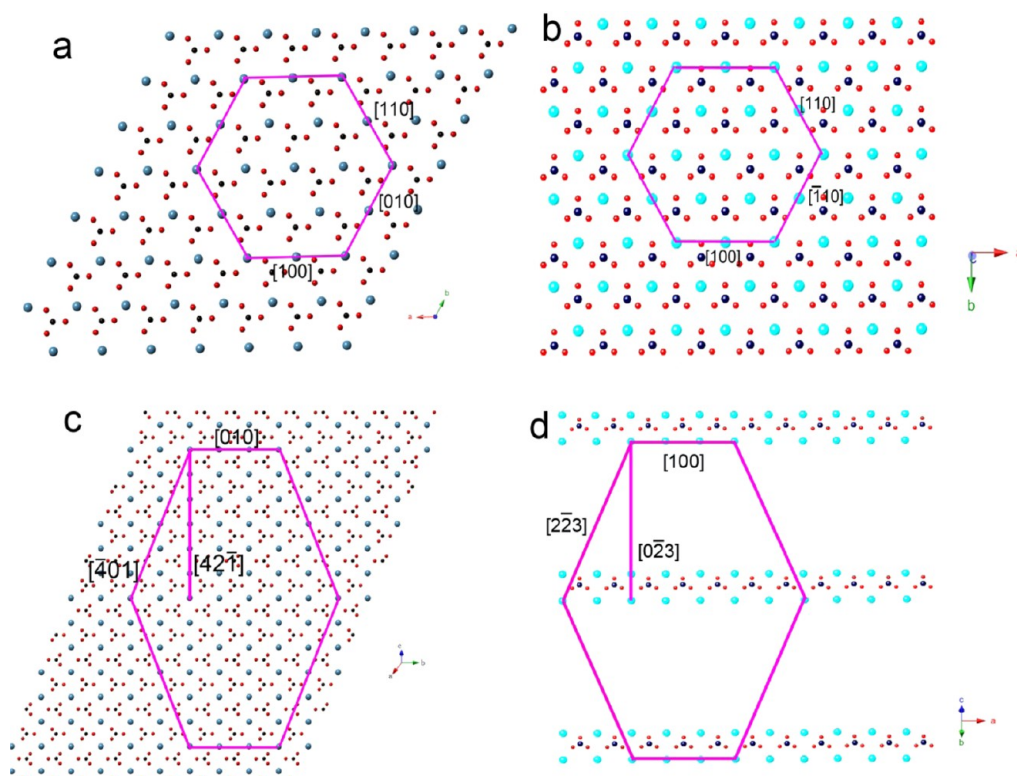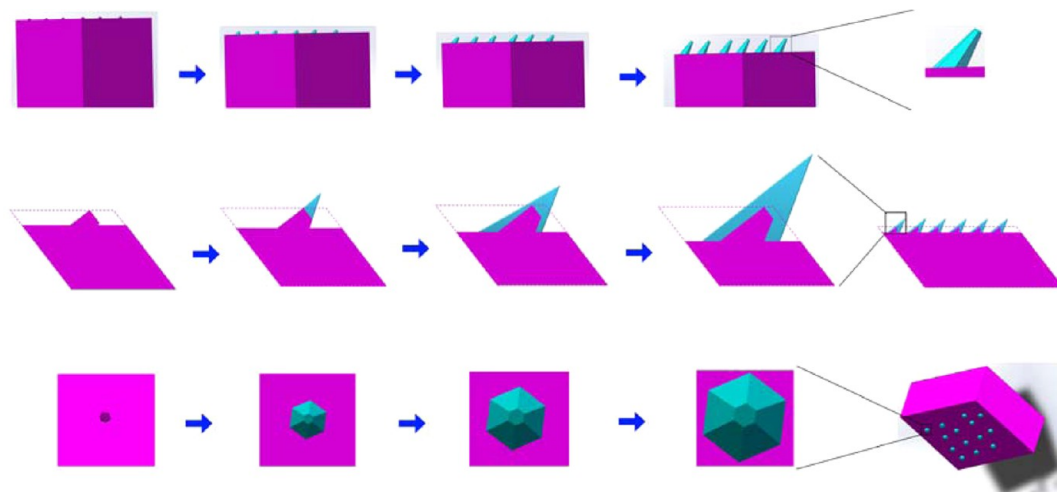
Scheme 1. Formation Process of Ca-Doped Strontianite-Calcite Hybrid Micropillars via Oriented Dissolution of Calcite and Heteroepitaxial Growth of Ca-Doped Strontianite on Calcite Substrate Is Proposed from Different Directions: (a) Side View, (b) Longitudinal Cross Section, (c) Top View

Figure 8. Atomic structures of calcite (001), (104) and strontianite (001), (032) planes. (a) calcite (001) face, (b) strontianite (001) face, (c) calcite (104) face, (d) strontianite (032) face. The four elements, O, C, Ca, and Sr, are exhibited by using spheres in red, black, dark blue, and bright blue, respectively. To compare and show the lattice steps for calcite and strontianite on different (*hkl*) planes, pink hexagons were added to the atomic structures.

basis of the above experimental results, a formation mechanism is proposed for the formation process of Ca-doped strontianite–calcite hybrid micropillars according to the detailed characterizations and the time sequence analysis of the Ca-doped strontianite micropillars (Scheme 1, eq 1). First, calcite hillocks with a long axis along [001] of calcite form on calcite substrate due to oriented dissolution of calcite in the mixed solvents of water and ethanol, similar to the formation of the calcite microneedles in our previous work.[32,33] Second, nucleation and heteroepitaxial growth of Ca-doped strontianite

along the [001] direction may start on the (001) plane of the calcite hillocks, while calcite substrates dissolve at the same time. Because of the dissolution of calcite in undersaturated solution, the local concentrations of CO_3^{2-} and the super-saturation degree for strontianite in the diffusion layer of calcite substrate are higher than that in the bulk solution. Therefore, the nucleation of strontianite on the calcite substrate is easier than that in the bulk solution. The distances of Sr atoms along [100], [110], and [$\bar{1}$10] on the (001) face of strontianite are 5.09, 4.89, and 4.89 Å, very close to the distances of Ca atoms

along ⟨100⟩ steps, (4.99 Å) on (001) face of calcite, with a mismatch about 2.0% (Figure 8a,b and Table S2). The distance of Sr atoms along the [100] step is a bit larger than that of Ca atoms along [100] of calcite, while the distances of Sr atoms along the [110] and [$\bar{1}$10] steps are slightly smaller than those of Ca atoms along the [010] and [110] steps. The stretch and compression along different directions may contribute to the proceeding of heteroepitaxial growth of strontianite on calcite. Third, the strontianite can further nucleate and grow on the calcite (104) plane via secondary nucleation and epitaxial growth. It can be seen that the strontianite micropillars are grown on flat calcite (104) substrate, and the growth interface is almost parallel to the (104) plane of calcite according to the SEM and TEM images (Figures 1 and 5). According to the atomic structures of calcite (104) plane and strontianite (032) plane, both of the distances and angles of the ⟨010⟩ and ⟨$\bar{4}$01⟩ of calcite are very close to those for the ⟨100⟩ and ⟨2$\bar{2}$3⟩ of stronthianite, with lattice misfits less than 2.0% (Figure 8c,d and Table S2). On the other hand, one can see a clearly curved line between the strontianite micropillars and calcite substrate with a perfect connection from the TEM image in Figure 5d. Therefore, more than one growth face probably exists for the heteroepitaxial growth of strontianite on calcite. We propose that new epitaxial growth frontiers of strontianite might form step by step on the circumference of the strontianite micropillars on the faces parallel to [010] of calcite, including (001) and (104) planes, according to the Volmer−Weber mode, during the dissolution of calcite. Diffusion rates and supersaturation degree are important factors for the dissolution of one mineral and the heteroepitaxial growth of a second mineral in aqueous solution.

The principal mechanism of strain relief for heteroepitaxial growth is the formation of three-dimensional islands either directly on a bare substrate (Volmer−Weber growth mode) or following the formation of an initially flat wetting layer (Stranski−Krastanov growth mode).[36] Considering the truth that no flat wetting layer of strontianite could form on calcite substrate since the calcite substrate dissolution continues while the strontianite micropillars epitaxially grow on calcite substrate, the Volmer−Weber mode may be more appropriate for the heteroepitaxial growth of Ca-doped strontianite micropillars on calcite substrate.

Owing to the relatively high concentration of Ca^{2+} in the diffusion layer of calcite substrate and the close atom sizes of Ca and Sr,[31] it is energetically and dynamically preferred for the occlusion of Ca in the strontianite during the epitaxial growth of strontianite on calcite substrate. It was pointed out that at ambient pressure and temperature, Ca^{2+} ions may exist in the strontianite structure in the Ca-poor strontium carbonate.[37] On the other hand, it happens very often for the occlusion of Sr in aragonite in the biogenic minerals.[38]

CONCLUSION

Herein, the heteroepitaxial growth of aragonite-type polymorph, strontianite, on calcite was investigated in detail. Ordered single crystalline calcium-doped strontianite−calcite hybrid micropillar arrays along the c axes of the two crystalline phases were prepared on calcite substrates via heteroepitaxial growth and oriented dissolution. The crystalline planes for the epitaxial growth frontier and the growth interface of the two carbonate minerals were investigated by using TEM and SEM analysis in this strontianite−calcite system. The lattices of strontianite and calcite match well at the growth interface since the two kinds of crystals have at least two pairs of crystal faces with lattice spacings and angles with small misfits (<2.3%). This work provides a novel strategy to synthesize arrays of single crystalline 1D hybrid materials with well connected crystal interface and complicated structures. The well ordered crystalline calcium-doped strontianite-calcite hybrid micropillar arrays might be used in drug delivery, as surfaces with special wettability, or as templates for other functional materials.

ASSOCIATED CONTENT

Ⓢ Supporting Information

SEM images for the transverse cross sections and EDS analysis results for the Ca-doped strontianite-calcite hybrid micropillars, influences of concentrations and temperatures, the XRD data of standard strontianite (JCPDS 05-0418) and Ca-doped strontianite-calcite hybrid micropillars, as well as the distance data of Ca and Sr atoms along different steps on different calcite and strontianite planes. This material is available free of charge via the Internet at http://pubs.acs.org.

AUTHOR INFORMATION

Corresponding Authors
*(Y.M) E-mail: yurong.ma@pku.edu.cn.
*(B.L) E-mail: binli@gxu.edu.cn.
Notes
The authors declare no competing financial interest.

ACKNOWLEDGMENTS

REFERENCES

(1) Markov, I.; Stoyanov, S. *Contemp. Phys.* **1987**, *28*, 267−320.
(2) Volmer, M.; Weber, A. *Z. Phys. Chem.* **1926**, *119*, 277−301.
(3) Eaglesham, D. J.; Cerullo, M. *Phys. Rev. Lett.* **1990**, *64*, 1943−1946.
(4) Fan, Z. Y.; Kapadia, R.; Leu, P. W.; Zhang, X. B.; Chueh, Y. L.; Takei, K.; Yu, K.; Jamshidi, A.; Rathore, A. A.; Ruebusch, D. J.; Wu, M.; Javey, A. *Nano Lett.* **2010**, *10*, 3823−3827.
(5) Medeiros-Ribeiro, G.; Bratkovski, A. M.; Kamins, T. I.; Ohlberg, D. A. A.; Williams, R. S. *Science* **1998**, *279*, 353−355.
(6) Silly, F.; Castell, M. R. *Phys. Rev. Lett.* **2005**, *94*, 046103.
(7) Shin, J. C.; Kim, K. H.; Yu, K. J.; Hu, H. F.; Yin, L. J.; Ning, C. Z.; Rogers, J. A.; Zuo, J. M.; Li, X. L. *Nano Lett.* **2011**, *11*, 4831−4838.
(8) Segura-Ruiz, J.; Martinez-Criado, G.; Denker, C.; Malindretos, J.; Rizzi, A. *Nano Lett.* **2014**, *14*, 1300−1305.
(9) Zhu, Y.; Zhou, Y.; Utama, M. I. B.; de la Mata, M.; Zhao, Y. Y.; Zhang, Q.; Peng, B.; Magen, C.; Arbiol, J.; Xiong, Q. H. *Nanoscale* **2013**, *5*, 7242−7249.
(10) Zhong, Z. Y.; Schwinger, W.; Schaffler, F.; Bauer, G.; Vastola, G.; Montalenti, F.; Miglio, L. *Phys. Rev. Lett.* **2007**, *98*, 176102.
(11) Putnis, A. *Science* **2014**, *343*, 1441−1442.
(12) Putnis, A. In *Thermodynamics and Kinetics of Water-Rock Interaction*; Oelkers, E. H., Schott, J., Eds.; Mineralogical Society of America: Chantilly, 2009; Vol. 70, pp 87−124.
(13) Putnis, C. V.; Ruiz-Agudo, E. *Elements* **2013**, *9*, 177−182.
(14) Sethmann, I.; Wang, J. W.; Becker, U.; Putnis, A. *Cryst. Growth Des.* **2010**, *10*, 4319−4326.
(15) Pimentel, C.; Pina, C. M.; Gnecco, E. *Cryst. Growth Des.* **2013**, *13*, 2557−2563.

(16) Xu, M.; Kovarik, L.; Arey, B. W.; Felmy, A. R.; Rosso, K. M.; Kerisit, S. *Geochim. Cosmochim. Acta* **2014**, *134*, 221−233.

(17) Kim, I. W.; Robertson, R. E.; Zand, R. *Adv. Mater.* **2003**, *15*, 709−712.

(18) Wu, W. K.; zhang, Y. Z.; Li, B.; Ma, Y. R. *Acta Phys. Chim. Sin.* **2015**, *31*, 189−198.

(19) Homeijer, S. J.; Barrett, R. A.; Gower, L. B. *Cryst. Growth Des.* **2010**, *10*, 1040−1052.

(20) Balz, M.; Therese, H. A.; Kappl, M.; Nasdala, L.; Hofmeister, W.; Butt, H. J.; Tremel, W. *Langmuir* **2005**, *21*, 3981−3986.

(21) Cao, M. H.; Wu, X. L.; He, X. Y.; Hu, C. W. *Langmuir* **2005**, *21*, 6093−6096.

(22) Zhang, Y. Y.; Liu, J. L.; Zhu, Y. X.; Shang, Y.; Yu, M.; Huang, X. *J. Mater. Sci.* **2009**, *44*, 3364−3369.

(23) Ma, M. G.; Zhu, Y. J. *J. Nanosci. Nanotechnol.* **2007**, *7*, 4552−4556.

(24) Xu, S. J.; Wu, P. Y. *CrystEngComm* **2014**, *16*, 1311−1321.

(25) Rautaray, D.; Sainkar, S. R.; Sastry, M. *Langmuir* **2003**, *19*, 888−892.

(26) Rautaray, D.; Sanyal, A.; Adyanthaya, S. D.; Ahmad, A.; Sastry, M. *Langmuir* **2004**, *20*, 6827−6833.

(27) Taylor, J. D. *Palaeontology* **1973**, *16*, 519−534.

(28) Checa, A. G.; Rodriguez-Navarro, A. *Proc. R. Soc. B* **2001**, *268*, 771−778.

(29) Checa, A. G.; Rodriguez-Navarro, A. B. *Biomaterials* **2005**, *26*, 1071−1079.

(30) Olson, I. C.; Blonsky, A. Z.; Tamura, N.; Kunz, M.; Pokroy, B.; Romao, C. P.; White, M. A.; Gilbert, P. *J. Struct. Biol.* **2013**, *184*, 454−463.

(31) Shirota, Y.; Niki, K.; Shindo, H. *J. Cryst. Growth* **2011**, *324*, 190−195.

(32) Meng, R. J.; Ma, Y. R.; Long, X.; Yang, D.; Qi, L. M. *CrystEngComm* **2013**, *15*, 8867−8873.

(33) Long, X.; Meng, R. J.; Wu, W. K.; Ma, Y. R.; Yang, D.; Qi, L. M. *Chem.—Eur. J.* **2014**, *20*, 4264−4272.

(34) Erdemoglu, M.; Canbazoglu, M. *Hydrometallurgy* **1998**, *49*, 135−150.

(35) Guo, G. L.; Yan, G. W.; Wang, L.; Huang, J. H. *Mater. Lett.* **2008**, *62*, 4018−4021.

(36) Ratto, F.; Rosei, F. *Mater. Sci. Eng. R* **2010**, *70*, 243−264.

(37) Kulik, D. A.; Vinograd, V. L.; Paulsen, N.; Winkler, B. *Phys. Chem. Earth* **2010**, *35*, 217−232.

(38) Finch, A. A.; Allison, N. *Geochim. Cosmochim. Acta* **2003**, *67*, 4519−4527.